Research Square

Preprints are preliminary reports that have not undergone peer review.
They should not be considered conclusive, used to inform clinical practice,
or referenced by the media as validated information.

Purification, Characterization, and Green Synthesis of ZnO Nanoparticles Using Purified Lignin Peroxidase from Fusarium odoratissimum for Environmental Remediation

Neki Borang
North Eastern Regional Institute of Science and Technology (NERIST) Nirjuli
Antarikha Dutta
North Eastern Regional Institute of Science and Technology (NERIST) Nirjuli
Meera Yadav
drmeerayadav@rediffmail.com

North Eastern Regional Institute of Science and Technology (NERIST) Nirjuli

Research Article

Keywords: Fusarium odoratissimum, ligninolytic peroxidase, enzyme purification, green synthesis, zinc oxide nanoparticles, wastewater treatment, BOD, COD

Posted Date: October 30th, 2026

DOI: https://doi.org/10.21203/rs.3.rs-10904867/v1

License: This work is licensed under a Creative Commons Attribution 4.0 International License.
Read Full License

Additional Declarations: No competing interests reported.

Purification, Characterization, and Green Synthesis of ZnO Nanoparticles Using Purified Lignin Peroxidase from *Fusarium odoratissimum* for Environmental Remediation

Neki Borang[1], Antarikha Dutta[1], Meera Yadav[1]*

[1]*Department of Chemistry, North Eastern Regional Institute of Science and Technology (NERIST) Nirjuli, AP- 791109, India.*

Neki Borang
Email: nekiborang24@gmail.com
ORCID ID: 0009-0003-3817-2748

Antarikha Dutta
Email: Antarikhadutta123@gmail.com
ORCID ID: 0009-0000-8782-1749

Corresponding Author:

Dr. Meera Yadav*
Email: drmeerayadav@rediffmail.com
ORCID ID: 0000-0002-8326-6810

Associate Professor
Department of Chemistry
North Eastern Regional Institute of Science and Technology (NERIST)
Nirjuli, Arunachal Pradesh – 791109, India

Abstract

The present study investigated the production, purification, and application of lignin peroxidase (LiP) from *Fusarium odoratissimum* for enzyme-assisted green synthesis of zinc oxide nanoparticles (ZnO NPs). LiP was produced using agro-waste substrates and purified through sequential purification steps, resulting in an 18.55-fold increase in specific activity, with a final specific activity of 13.14 U mg^{-1} and 17.73% recovery. The purified LiP was subsequently employed for ZnO NP synthesis. The synthesized ZnO NPs were characterized using UV–Vis spectroscopy, FTIR, FESEM, EDS, dynamic light scattering, zeta potential analysis, particle-size analysis, and XRD. The characterization results supported the formation of crystalline ZnO nanoparticles and the association of surface functional groups with the nanoparticles. EDS analysis showed Zn and O contents of 82.66 and 17.34 wt%, respectively. The ZnO NPs demonstrated concentration- and contact-time-dependent treatment efficiency toward Dikrong River water, achieving approximately 96.8% BOD and 55.0% COD removal at the highest tested dose. The nanoparticles also exhibited radical-scavenging activity in ABTS and DPPH assays, with greater apparent activity than the extracellular enzyme extract under the tested conditions. Overall, the findings provide a proof-of-concept for LiP-assisted green synthesis of ZnO NPs and highlight their potential for sustainable environmental applications.

Keywords: *Fusarium odoratissimum*; lignin peroxidase; enzyme purification; green synthesis; zinc oxide nanoparticles; wastewater treatment; BOD; COD.

Introduction

Enzymes are highly efficient biocatalysts that regulate numerous biochemical transformations and contribute significantly to nutrient cycling and ecosystem sustainability. Among oxidoreductases, ligninolytic enzymes have attracted considerable attention because of their ability to catalyse complex redox reactions involved in the degradation of recalcitrant aromatic compounds (Thulasisingh et al., 2024; Wesenberg et al., 2003; Hashempour et al., 2025; Shi et al., 2025). Immobilized LiP systems have also demonstrated considerable potential for environmental remediation, with LiP-based cross-linked enzyme aggregates showing effective degradation of textile dyes in contaminated aqueous systems (Parveen et al., 2021). Lignin peroxidase (LiP; EC 1.11.1.14) is one of the most powerful extracellular heme-containing oxidoreductases, utilizing hydrogen peroxide (H_2O_2) to oxidize a broad spectrum of high-redox-potential substrates through long-range electron transfer mechanisms. Owing to its exceptional catalytic versatility, LiP has recently emerged as a promising biocatalyst for green nanobiotechnology, particularly in the sustainable synthesis of metal and metal oxide nanoparticles (Biko et al., 2020; Singh et al., 2021). Zinc oxide nanoparticles (ZnO NPs) have attracted considerable attention because of their unique optical, catalytic, antimicrobial, and photocatalytic properties, making them suitable for applications in environmental remediation, biosensing, agriculture, and biomedicine (Rani & Shanker, 2022). Conventional chemical and physical methods for ZnO nanoparticle synthesis frequently require elevated temperatures, hazardous chemicals, and toxic stabilizing agents, thereby raising environmental concerns and production costs. Consequently, biological approaches using microorganisms, plant extracts, and purified enzymes have emerged as more sustainable alternatives, enabling nanoparticle formation under relatively mild conditions while reducing the use of hazardous reagents and generation of undesirable by-products (Sharma et al., 2020; Gomaa, 2022; Murali et al., 2023; Borang et al., 2026). Although several studies have reported fungal- and microbial-mediated biosynthesis of ZnO nanoparticles, many of these approaches rely on crude culture filtrates or complex extracellular mixtures, making it difficult to determine the specific contribution of individual enzymes to nanoparticle formation. In biological ZnO synthesis, Zn^{2+} ions undergo hydrolysis followed by nucleation and crystal growth, while enzymes and associated biomolecules may contribute to precursor transformation, surface binding, nucleation, and stabilization. Therefore, the use of a defined purified enzyme system is important for better understanding the role of individual biocatalysts in ZnO nanoparticle formation.

Previous studies have demonstrated the ability of purified LiP to mediate the synthesis of metallic nanoparticles, including AgNPs and CuNPs, whereas ZnO synthesis has been reported mainly using whole fungal systems, extracellular filtrates, or enzymes other than LiP. For example, purified LiP has been employed for AgNP synthesis, while LiP-associated CuNP synthesis has also been reported using a different microbial source. In contrast, fungal-mediated ZnO synthesis has predominantly involved *Phanerochaete chrysosporium* or other complex biological systems, in which the specific contribution of LiP cannot be clearly distinguished. More recently, purified α-amylase has been used for ZnO nanoflower synthesis, demonstrating the feasibility of purified-enzyme-mediated ZnO formation but involving an enzyme unrelated to ligninolytic peroxidases. These studies collectively indicate that, although

enzyme-mediated nanoparticle synthesis is established, a defined purified LiP-mediated route for ZnO nanoparticle synthesis remains comparatively less explored. A comparison of representative enzyme- and fungus-mediated nanoparticle synthesis studies is presented in Table 1.

Sl. No.	Biological system	NP	Key feature	Application	Key distinction	Study
1	*Acinetobacter* sp. LiP	AgNPs	Purified LiP-mediated synthesis	Nanoparticle synthesis	AgNPs rather than ZnO; bacterial LiP	Singh et al. (2017)
2	*P. chrysosporium*	ZnO	Whole fungal filtrate	Antimicrobial	Purified LiP was not isolated as the synthesis mediator	Sharma et al., (2021a, 2021b)
3	*A. rupiensis* LiP	CuNPs	LiP-mediated synthesis	Antimicrobial	CuNPs rather than ZnO; different LiP source	Sus et al. (2024)
4	α-Amylase	ZnO	Purified enzyme-mediated synthesis	Photocatalytic/ antimicrobial	Uses α-amylase rather than ligninolytic LiP	Mazumder et al. (2024)

As outlined in Table 1, earlier research shows that purified LiP has been utilized in producing AgNPs and CuNPs and in the synthesis of ZnO from fungal filtrates or other than LiP enzymes. Still, the results of these studies differ from that of the present work by composition of the nanoparticles, biological source of the LiP enzyme used and also the method of research execution. In this study purified LiP from *Fusarium odoratissimum* was utilized for producing ZnO nanoparticles. The produced ZnO nanoparticles were characterized by several physicochemical methods to prove their suitability for environmental remediation. Therefore, it can be stated that the research presented in this study is novel since it presents the established *F. odoratissimum*-based LiP-ZnO synthesis system, and also describes the use of purified enzyme in producing ZnO nanoparticles for environmental remediation purposes. Thus, the aim of the present study is to purify and characterize LiP from *Fusarium odoratissimum*, and use it for the green synthesis of ZnO nanoparticles. The synthesized ZnO nanoparticles were adequately characterized and analyzed for their properties and applicability. This approach provides a more defined enzyme-mediated alternative to conventional chemical synthesis and whole-fungal ZnO nanoparticle production.

2. Materials and Methods

2.1 Chemicals

Analytical grade reagents were obtained from CDH (New Delhi), Loba Chemie (Mumbai), and SRL (Mumbai).

2.2 Isolation and Identification of Fungal Strain

Soil samples from contaminated sites at Naharlagun (Arunachal Pradesh), Harmutty (Assam), and NERIST campus (Nirjuli, Arunachal Pradesh) were serially diluted and spread on potato dextrose agar (PDA). Distinct colonies were purified by repeated streaking and maintained at 4°C on PDA slants. The most efficient ligninolytic isolate was identified through ITS rDNA sequencing as *Fusarium odoratissimum*.

2.3 LiP Production and Purification

2.3.1 Fungal cultivation and medium composition

Fusarium odoratissimum was cultivated in a modified Tien and Kirk medium (pH 4.5) (Tien & Kirk, 1984) freshly prepared in 1 L of double-distilled water. The medium contained glucose (10 g), ammonium tartrate (1.32 g), KH_2PO_4 (0.2 g), $MgSO_4 \cdot 7H_2O$ (50 mg), $CaCl_2$ (10 mg), and thiamine-HCl (10 µg). Additionally, 1 mL of freshly prepared trace element solution was added, containing $MgSO_4 \cdot 7H_2O$ (3 g), $MnSO_4 \cdot H_2O$ (0.5 g), NaCl (1 g), $FeSO_4 \cdot 7H_2O$ (100 mg), $CoCl_2 \cdot 6H_2O$ (185 mg), $CaCl_2$ (80 mg), $ZnSO_4 \cdot 7H_2O$ (180 mg), $CuSO_4 \cdot 4H_2O$ (10 mg), $AlK(SO_4)_2$ (10 mg), H_3BO_3 (10 mg), $Na_2MoO_4 \cdot 2H_2O$ (12 mg), and nitrilotriacetate (1.5 g). The medium was sterilized by autoclaving at 121 °C for 30 min, and the pH was maintained using 20 mM sodium succinate buffer.

2.3.2 Substrate induction and culture conditions

In order to enhance ligninolytic enzyme production through LiP induction, the following lignin-rich agricultural by-products were used as additional substrates for carbon: rice husks, wheat straws, sawdust, coconut husks, and molasses. Each substrate was thoroughly washed with distilled water, and the solids were dried in a convection oven at 60 °C (140 °F), ground, and screened to produce uniform-size particles (1–2 mm) before the onset of the experiment. The optimum substrate concentration was found to be 0.5 g of dry residue/20 mL of media based on previous literature and preliminary optimisation approaches for ligninolytic enzyme production in submerged fermentation. Each substrate was supplemented individually into sterilised 100 mL Erlenmeyer flasks containing 20 mL of media. Each flask received an inoculum of 1 cm^2 mycelial agar plugs from the actively growing peripheral region derived from 5–7-day-old PDA culture of *Fusarium odoratissimum* and were incubated at 28±2 °C with shaking at 120 rpm (Pointing, 2001).

All experiments were performed in triplicate (n = 3) under the same conditions. The 100 mL Erlenmeyer flasks containing 20 mL of media were used for the fermentation process. For inoculum standardization, all inoculated test flasks contained equal size (1 cm^2) mycelial agar plugs from actively growing parent cultures as inoculum.

2.3.3 Crude enzyme extraction and ammonium sulphate precipitation

After incubating for 3-5 days, at which point maximum LiP activity was detected, the culture broth was filtered through sterile muslin cloth to separate the liquid from the fungal biomass. The 80% ammonium sulphate saturation level was selected based on preliminary optimization experiments and previously reported purification protocols for fungal LiPs, where maximum enzyme recovery was observed within this precipitation range. The precipitated proteins were separated from the enzymes by centrifuging at a speed of 10,000 rpm for 20 minutes; these pellets were then resuspended in sodium succinate buffer (10mM; pH 5.0).

2.3.4 Dialysis and ion-exchange chromatography

The enzymes were subsequently dialyzed overnight at 4 °C against 1000 × volume of sodium succinate buffer (pH 5.0). The dialyzed enzyme solution was loaded onto a DEAE-cellulose ion-exchange chromatography column (1.5 × 20 cm) pre-equilibrated with 10 mM sodium succinate buffer (pH 5.0). Elution was carried out using a linear NaCl gradient (0–200 mM) at a flow rate of 1 mL min^{-1}, and fractions of 2 mL were collected. Protein elution was monitored at 280 nm, while LiP activity was determined by monitoring veratryl alcohol oxidation at 310 nm. Fractions showing maximum LiP activity were pooled and stored at 4 °C for further purification and characterization (Bouacem et al., 2018; Wheelwright, 1991).

2.3.5 Protein quantification

The protein concentration was determined using the following method by Lowry et al (1951), which involved using Bovine Serum Albumin (BSA) for standardization. Enzyme aliquots were treated with alkaline copper reagent, allowed to incubate, and reacted with Folin-Ciocalteu reagent. Absorbance was recorded at a wavelength of 750 nm.

2.3.6 SDS-PAGE analysis

The purity and molecular weight of LiP were determined using SDS-PAGE according to Laemmli (1970), using a 12% resolving gel.

2.4 Optimization and physicochemical characterization of LiP

The optimization of the production of LiP enzyme production was conducted on multiple agro-residues to be used in submerged fermentation to grow ligninolytic enzymes (Kumar and Chandra, 2020; Pointing, 2001). The effects of pH (2.0−8.0), temperature (20−60 °C), and substrate concentration were determined by standard optimization procedures (Singh et al., 2022). Nutritional optimization through the addition of various carbon, nitrogen, sulphur, and phosphorus to the growth media was based on the nutritional composition of the growth medium used for production of ligninolytic enzymes (Elisashvili and Kachlishvili, 2009). For the physicochemical characterization, enzyme activities were evaluated across various pH ranges and temperature ranges, according to standard chemical characterization procedures (Worthington, 1993). Buffer concentration was assessed using sodium tartrate buffer (10−100 mM) as a buffer system.

2.5 Enzyme Assays and Characterization

LiP activity was assayed using 2 mM veratryl alcohol and 0.4 mM H_2O_2 in 50 mM sodium tartrate buffer (pH 3.0). The reaction mixture (1.0 mL) contained 800 µL buffer, 100 µL appropriately diluted enzyme, 50 µL veratryl alcohol (40 mM), and 50 µL H_2O_2 (8 mM). The reaction was initiated by the addition of H_2O_2, and veratraldehyde formation was monitored at 310 nm for 1 min using a 1-cm path length. A reagent blank without enzyme was used for background correction. LiP activity was calculated from the blank-corrected change in absorbance using ε = 9300 M^{-1} cm^{-1} according to the equation

$$\text{LiP activity (U/mL)} = \frac{\Delta A_{310}/\text{min} \times V_r \times DF \times 1000}{\varepsilon \times l \times V_e}$$

where ΔA_{310}/min is the blank-corrected change in absorbance per minute, V_r is the total reaction volume (mL), DF is the dilution factor, ε is the molar extinction coefficient (M^{-1} cm^{-1}), l is the path length (cm), and V_e is the enzyme volume (mL). One unit (U) was defined as the amount of enzyme required to oxidize 1 µmol of veratryl alcohol per minute under the assay conditions. Measurements were performed in triplicate. *n*-Propanol oxidation was additionally monitored at 290 nm using an extinction coefficient of ε = 26,600 M^{-1} cm^{-1}.

Kinetic parameters (K_m, V_{max}, K_{cat}) were determined from Michaelis-Menten and Lineweaver-Burk plots using the following equations:

$$1/V = (K_m/V_{max})\,(1/S) + 1/V_{max}$$

$$K_{cat} = V_{max}/[E_t]$$

where v = initial reaction rate, [S] = substrate concentration, [E] = enzyme concentration.

2.6 Synthesis of ZnO nanoparticles using purified LiP

ZnO nanoparticles were synthesized using purified LiP through an enzyme-mediated green synthesis approach (El-Saadony et al., 2024). Briefly, 1 mL of purified LiP (4.6 U enzyme activity and 0.35 mg protein) was mixed with 9 mL of 1 mM zinc nitrate hexahydrate [$Zn(NO_3)_2 \cdot 6H_2O$] under continuous stirring. The reaction mixture was incubated at 30 °C for 24 h at pH 5.0 under dark conditions with gentle shaking (120 rpm). Subsequently, the pH was gradually adjusted to 10.0 using 0.1 M NaOH, and the reaction mixture was further stirred for 2 h to facilitate the formation of ZnO nanoparticles. The precipitate obtained was separated by centrifugation for 15 minutes at 10,000 x g, then washed three times first with deionized water and then with absolute ethanol to eliminate excess salts and unbound molecules, and then dried for one night at 60 °C. The production of ZnO nanoparticles was monitored through the UV-Vis spectrometry, and their successful creation was confirmed through the characteristic peak of ZnO, appearing between 370-380 nm. The functional groups engaged in the generation and stabilization of the particles were determined through Fourier-transform infrared (FTIR) spectrometry, in the range of 4000-400 cm^{-1}. The morphology and surface characteristics of the synthesized nanoparticles were examined using field emission scanning electron microscopy (FESEM). The crystalline nature of the nanoparticles was investigated by X-ray diffraction (XRD) over a 2θ range of 20°–80°, while the elemental composition was confirmed using energy-dispersive X-ray spectroscopy (EDS) coupled with FESEM (Anuar et al., 2025; Nehru

et al., 2023). For FTIR analysis, dried samples of purified LiP and ZnO nanoparticles were mixed with KBr and scanned over the specified wavelength range. FESEM samples were prepared by mounting dried nanoparticle powder on conductive carbon tape followed by gold sputter coating prior to imaging.

2.7 Application of LiP-mediated ZnO nanoparticles for BOD and COD removal

2.7.1 Collection of river water samples

Water samples were collected from the Dikrong River, Arunachal Pradesh, India, using sterile high-density polyethylene (HDPE) bottles (2 L capacity). Prior to sample collection, the bottles were thoroughly washed with distilled water and rinsed with the river water at the sampling site. Samples were collected approximately 20–30 cm below the water surface to minimize contamination from surface debris. The collected samples were transported to the laboratory in an insulated ice box and stored at 4 °C until further analysis. Physicochemical analyses were initiated within 24 h of sample collection.

2.7.2 Treatment of river water using LiP-mediated ZnO nanoparticles

For each experiment, 100 mL of Dikrong River water was transferred into a 250 mL Erlenmeyer flask. LiP-mediated ZnO nanoparticles were added at different dosages (20, 40, 60, 80, and 100 mg). The reaction mixtures were agitated at 150 rpm using an orbital shaker at 28 ± 2 °C for predetermined contact times (20, 40, 60, 80, and 100 min). After treatment, the suspensions were centrifuged at 10,000 rpm for 10 min, and the supernatants were collected for BOD and COD analyses (Vignati et al., 2021).

2.7.3 Determination of biochemical oxygen demand (BOD)

The biochemical oxygen demand (BOD) was determined according to the Standard Methods for the Examination of Water and Wastewater (APHA, 2017). River water samples before and after nanoparticle treatment were transferred into 300 mL BOD bottles, and the dissolved oxygen (DO) concentration was measured using a calibrated dissolved oxygen meter. The bottles were incubated in the dark at 20 ± 1 °C for 5 days, after which the final DO was recorded. BOD was calculated as:

$$\text{BOD (mg/L)} = DO_{\text{initial}} - DO_{\text{final}}$$

The removal efficiency was calculated using:

$$\text{Removal (\%)} = \frac{C_0 - C_t}{C_0} \times 100$$

where C_0 is the initial BOD concentration and C_t is the final BOD concentration after treatment.

2.7.4 Determination of chemical oxygen demand (COD)

COD was measured using the closed reflux dichromate method (APHA, 2017). Briefly, 2.5 mL of treated and untreated river water samples were digested with potassium dichromate reagent

and sulfuric acid containing silver sulphate catalyst at 150 °C for 2 h. After cooling, absorbance was measured at 600 nm, and COD values were calculated from a calibration curve. The percentage COD removal was calculated using the same equation described above.

2.8 Radical-Scavenging Activity of LiP-mediated ZnO NPs

The radical-scavenging activity of the extracellular enzyme extract and LiP-mediated ZnO nanoparticles was evaluated using ABTS and DPPH assays. Different concentrations of the samples were incubated with $ABTS^{\bullet+}$ and DPPH solutions, and the absorbance was measured at 734 and 517 nm, respectively. Appropriate blanks and controls were included. Radical-scavenging activity was calculated as:

$$\text{Radical-scavenging activity (\%)} = [(A_0 - A_1)/A_0] \times 100$$

where A_0 is the absorbance of the control and A_1 is the absorbance of the sample. All measurements were performed in triplicate, and EC_{50} values were determined from concentration response curves.

2.9 Statistical Analysis

All experiments were performed in triplicate (n = 3), and results are expressed as mean ± standard deviation (SD). Statistical analysis was carried out using GraphPad Prism (version 8.0, GraphPad Software, San Diego, USA). One-way analysis of variance (ANOVA) was used to determine statistically significant differences among groups, followed by appropriate post hoc tests where applicable. Differences were considered statistically significant at $p < 0.05$.

3. Results and Discussion

3.1 Isolation, and identification of the fungal strain

Ligninolytic fungal strains were isolated from soil samples, and a high LiP –producing isolate was selected following preliminary screening. Fig.1 illustrates the macroscopic colony morphology of the selected isolate grown on agar medium, characteristic of *Fusarium odoratissimum*. Molecular identification based on ITS rDNA sequencing confirmed the taxonomic identity of the isolate as *Fusarium odoratissimum*, validating it as a LiP-producing strain (Supplementary File S1).

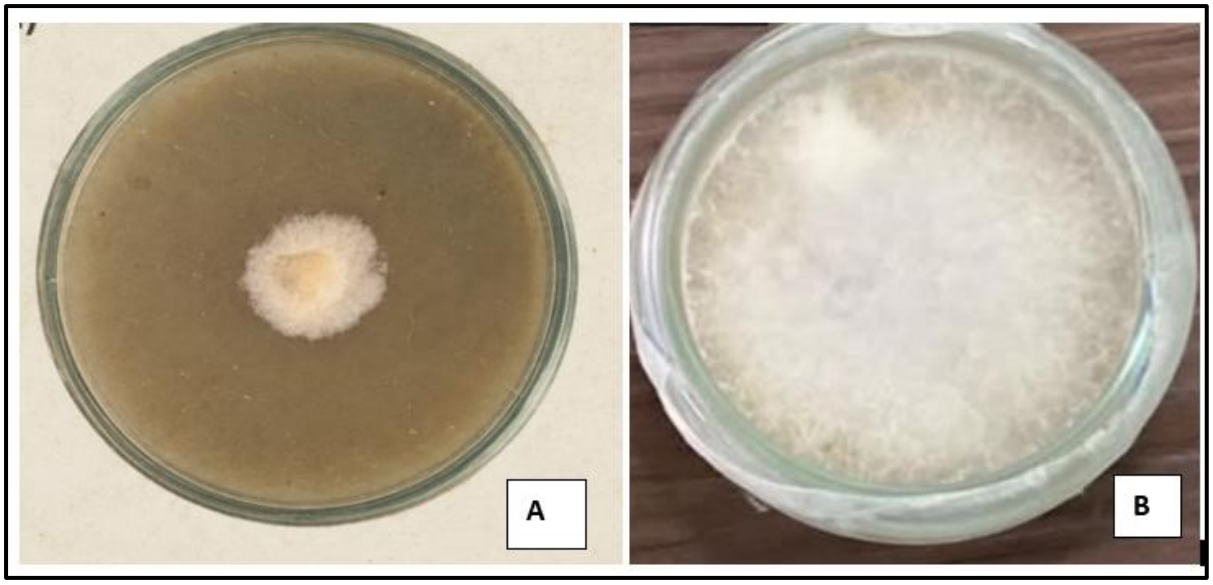


Fig. 1. Macroscopic colony morphology of *Fusarium odoratissimum* grown on agar medium. (a) Young colony showing initial mycelial growth; (b) mature colony exhibiting dense, white, cottony mycelial expansion.

3.2 Optimization Strategies for LiP under Physicochemical and Nutrient Parameters

Among different agro-residues tested, wheat straw showed the highest LiP production with peak 0.18 µmol min^{-1} on day 4, followed by rice husk 0.15 µmol min^{-1} and sawdust 0.14 µmol min^{-1} as illustrated in Fig 2. The enzyme yield from molasses and coconut husk was found to be relatively low. The highest production of LiP occurred at pH level of 3.0 and temperature of 30 °C, causing decrease in enzyme activity after that in all substrates tested, which indicate the effect of the nutrients and conditions on the production of ligninolytic enzymes.

Appropriate nutrient composition has an influence on LiP production by *Fusarium odoratissimum* in wheat straw medium presented in Fig. 3. The addition of glucose resulted in maximum enzyme yield at optimum concentration of 2.5 mg mL^{-1} and any further increase of this substance resulted in decrease in LiP production. Nitrogen concentration had optimum value of 1.5-2.0 mg mL^{-1} while excess amount decreases enzyme synthesis. Sulphur gave peak LiP yield at 2.5 mg mL^{-1} while phosphorus optimum was 1.5 mg mL^{-1}. All in all, moderate balancing concentrations of nutrients improved LiP production significantly while too much concentration had a negative effect on synthesis.

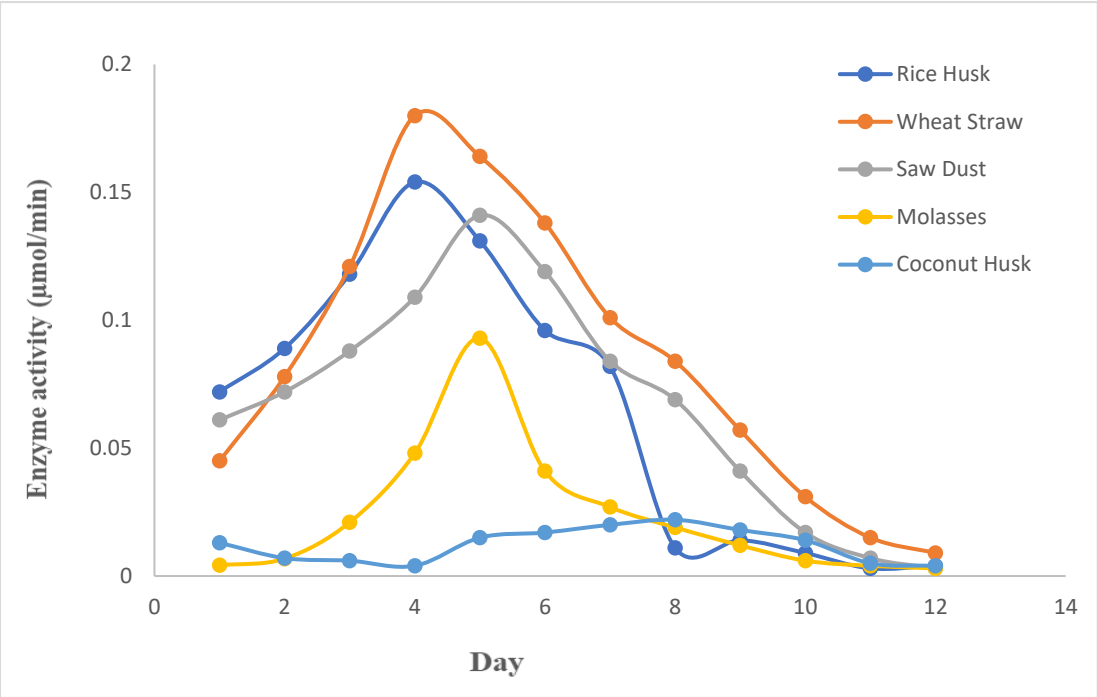


Fig. 2. Time-course of LiP production by the isolate using different agro-residues as substrates.

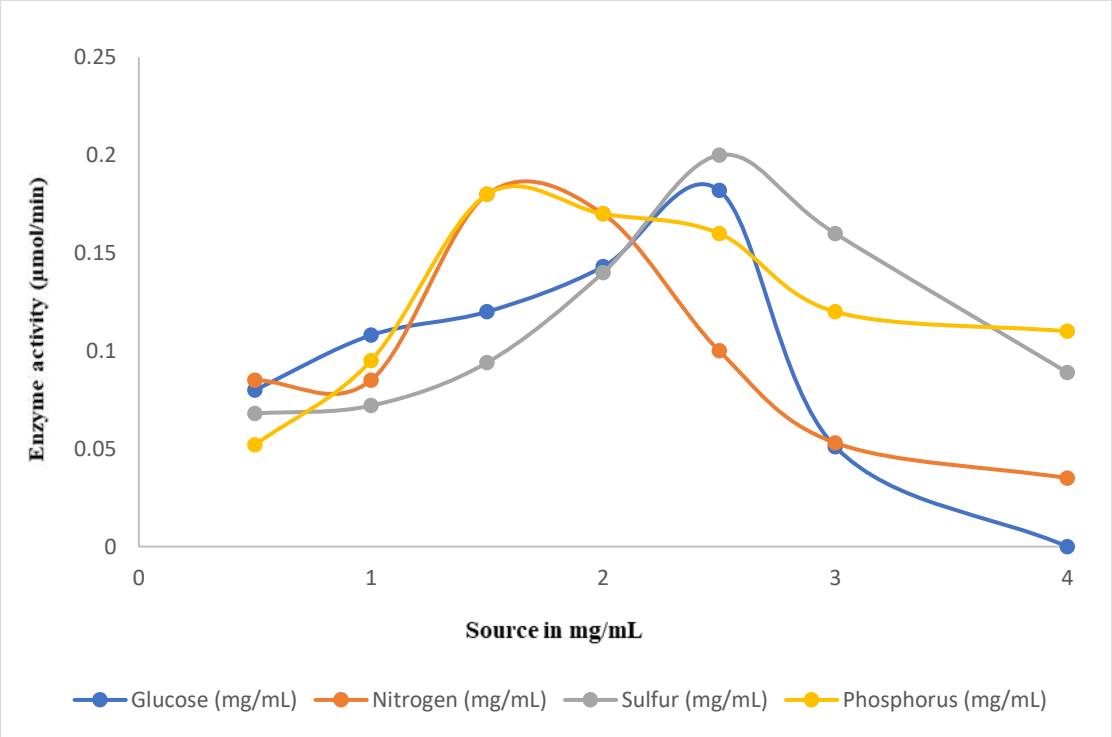


Fig. 3. Concentration-dependent effect of glucose, nitrogen, sulphur, and phosphorus on LiP production by *Fusarium odoratissimum* grown on wheat straw medium.

3.3 LiP Purification and SDS-PAGE Profiling

LiP from *Fusarium odoratissimum* was purified by sequential ammonium sulphate precipitation, dialysis, DEAE-cellulose ion-exchange chromatography, and sucrose gradient

centrifugation, as summarized in **Table 1.** The enzyme productivity increased from 0.71 U mg-1 in the crude extract to 13.14 U mg^{-1} in the purified fraction, representing an 18.55-fold increase in enzyme purity with the recovery of 17.73% of LiP from the total LiP in the crude extract. DEAE-cellulose chromatography produced a peak of LiP activity (Fig. 4). The SDS-PAGE results for the purified sample demonstrated one protein band at about 50 kDa which is in agreement with those documented in the literature for various isoforms of fungal LiP (Fig. 5). MALDI-TOF mass spectrometric analysis further supported the identification of the purified enzyme as LiP. The purified LiP obtained after sucrose gradient purification exhibited a specific activity of 13.14 U/mg, with 18.55-fold purification and 17.73% recovery. The peptide mass fingerprint obtained from the purified SDS-PAGE band showed a match with a LiP protein sequence comprising 374 amino acid residues, with a theoretical isoelectric point (pI) of 5.77. The purified enzyme exhibited a single protein band at approximately 43 kDa on SDS-PAGE (Fig. 5), indicating a high degree of purity.

1	MLWSNVIATS	VALAGVPSAL	GYPGMGEQMA	EIMSRQSAND	GFDSTELLGD
51	LQTLPDNQLT	PTASTTAWSA	PRLGTAACQK	DTCCVWQYIV	NDMVAEFKGS
101	SGRCTSWARR	AVRLGFHDAG	TWSKTTAAQG	LPGGADGSIC	TTDEINRADN
151	NGLQDICQKV	NGWYNTWNKQ	KGYPVSLADI	IQMGATVATV	VCPRGPRIKS
201	YVGRVDVAQA	GPPNLLPGVD	NSADDLIALF	RDKTIGPHSL	TALVGAHTTS
251	QQFFVNTSRA	GDPQDSTPTA	PEWQKFAGAG	GQKDWNEDFA	AGYIRLSLLG
301	VNNINKLTEC	TKVLPGGIPS	FTPNDQANVD	KWLNTADQSP	TAKKISDALH
351	AGQSLLGWLF	SLINGILGGL	KKTA		

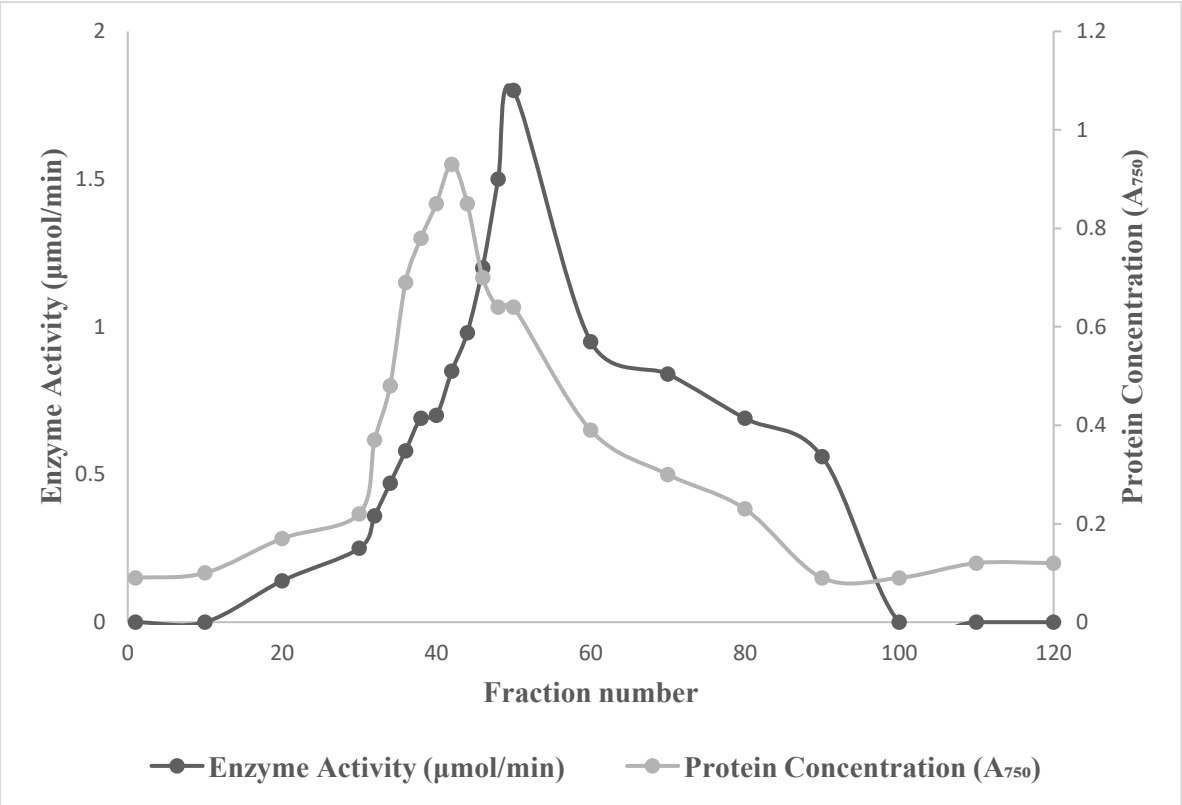


Fig. 4. DEAE-cellulose ion-exchange chromatographic profile of LiP produced by *Fusarium odoratissimum*, illustrating protein elution and enzymatic activity against veratryl alcohol under oxidative conditions.

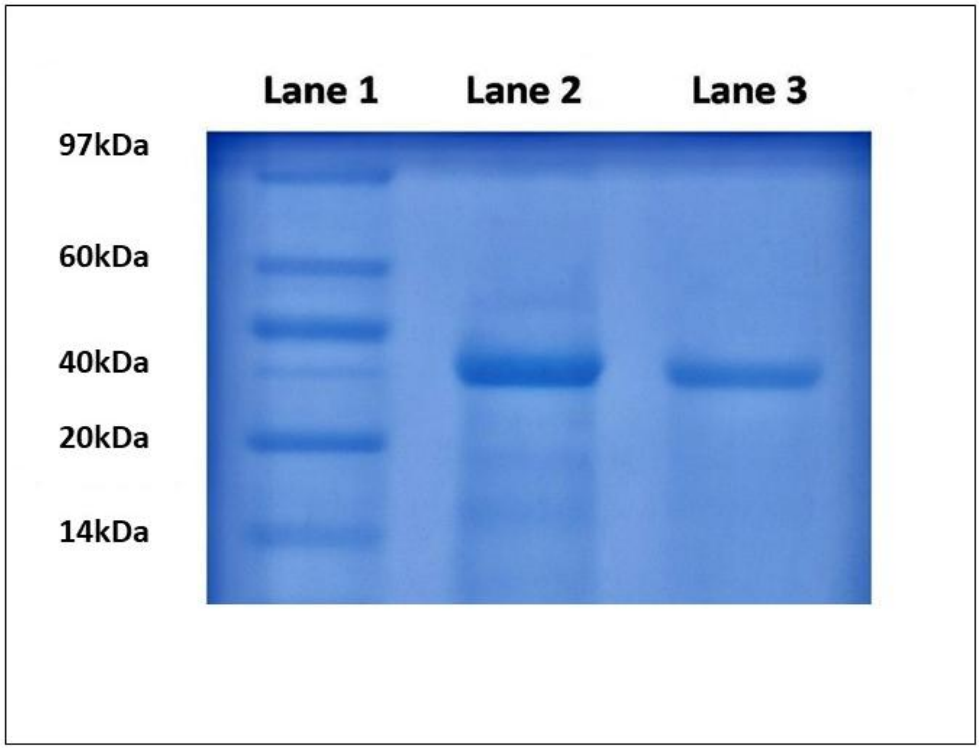


Fig. 5. SDS-PAGE of LiP purified from *Fusarium odoratissimum*: Lane 1 - molecular weight standards (kDa); Lane 2 - crude enzyme extract; Lane 3 - sucrose gradient-purified LiP showing a distinct single band at 50 kDa.

Table 1. Stepwise purification summary of LiP from *Fusarium odoratissimum*, involving ammonium sulphate-precipitation, dialysis, DEAE-cellulose chromatography, and sucrose gradient centrifugation.

Sl. No.	Step	Volume (mL)	Activity (U/mL)	Protein (mg/mL)	Total Activity (U)	Total Protein (mg)	Specific Activity (U/mg)	Purification Fold	% Recovery
1	Crude Enzyme	850	0.58	0.82	493	697	0.71	1	100
2	Ammonium Sulphate Conc.	25	3.4	2.9	85	72.5	1.17	1.65	17.24
3	Dialyzed Enzyme	35	2.5	1.8	87.5	63	1.39	1.96	17.75
4	DEAE Chromatography	50	1.8	0.94	90	47	1.91	2.69	18.25
5	Sucrose Gradient Purified	19	4.6	0.35	87.4	6.65	13.14	18.55	17.73

3.4 UPLC and QTOF-MS/MS Characterization

Using ULPC analysis, the purity of the purified LiP was evaluated in a UPLC chromatogram (Fig. 6), that displays a clear single peak with a corresponding retention time of 31.6-31.7 minutes, suggesting that this enzyme has gone through successful purification with a very high degree of purity as indicated by the lack of numerous secondary peaks suggesting low levels of contamination. Final confirmation of the successful purification was obtained using the analytical methods of QTOF-MS and MS/MS as shown in Fig. 7. The QTOF-MS spectrum displayed one of the most-significant ions at m/z 284.33, with many additional, but lower-mass fragment ions resulting from the dissociation of the original parent ion, or by electrospray dissociating the parent ion into many peptide fragments that constitute the heme-type LiP. Furthermore, based on the mass-spectrometric fragmentation pattern produced from our MS/MS analysis of the purified enzyme we can conclude that the identity and integrity of the purified enzyme are further-supported by previously reported fungal LiP results obtained via mass spectrometry.

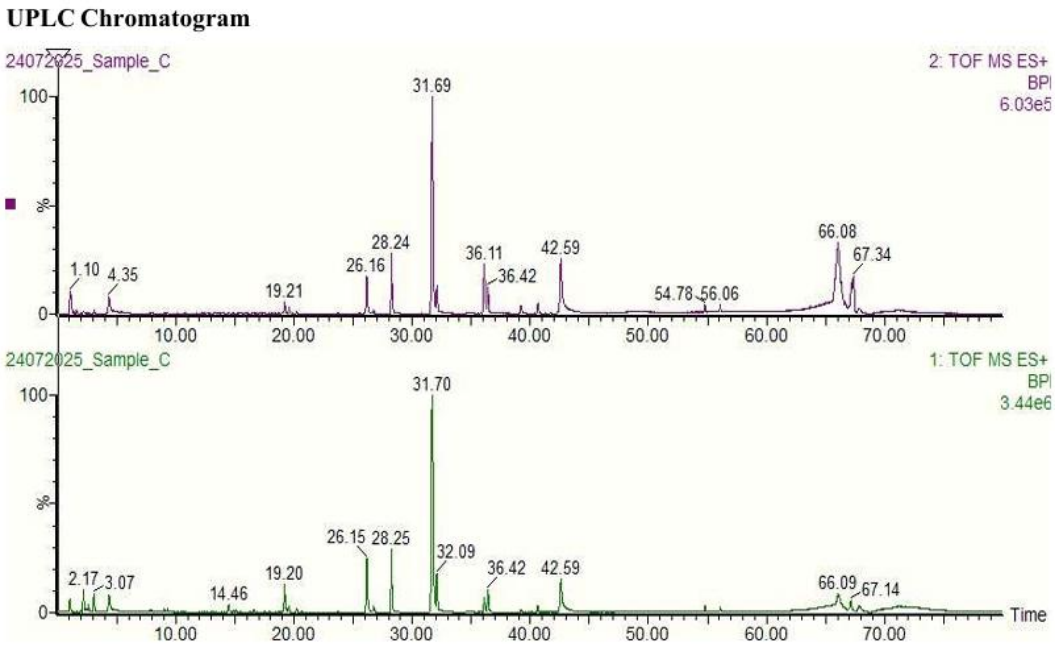


Fig. 6. UPLC–TOF MS total ion chromatograms of purified LiP in positive ion mode for (1) MS and (2) MS/MS.

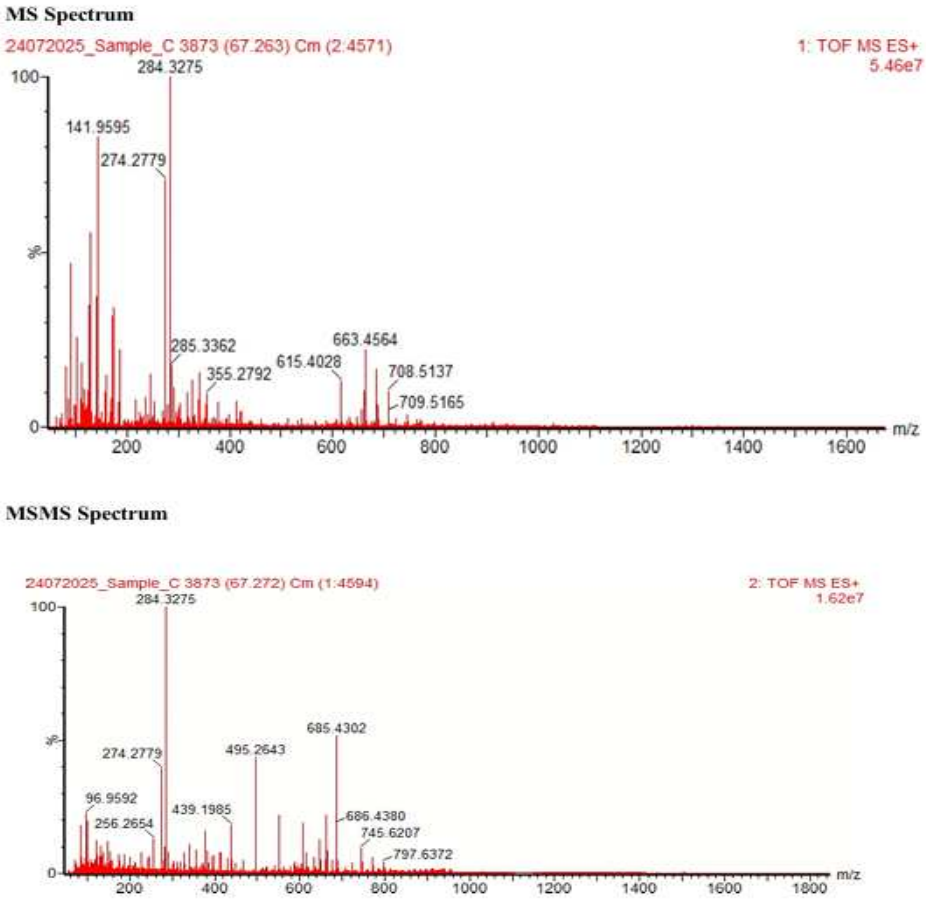
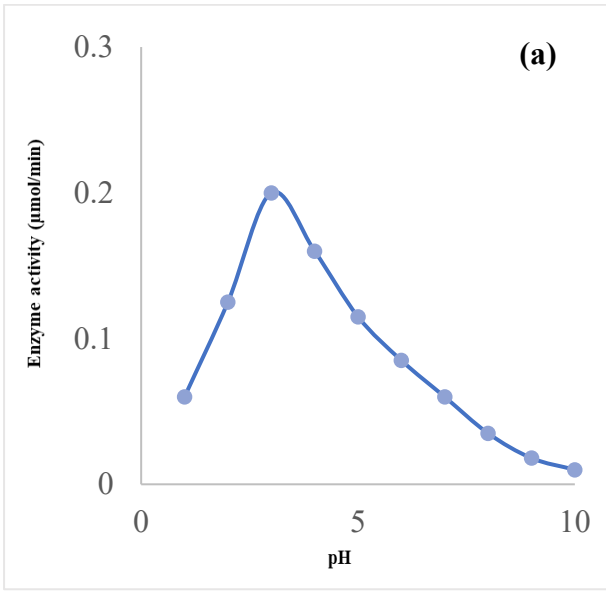
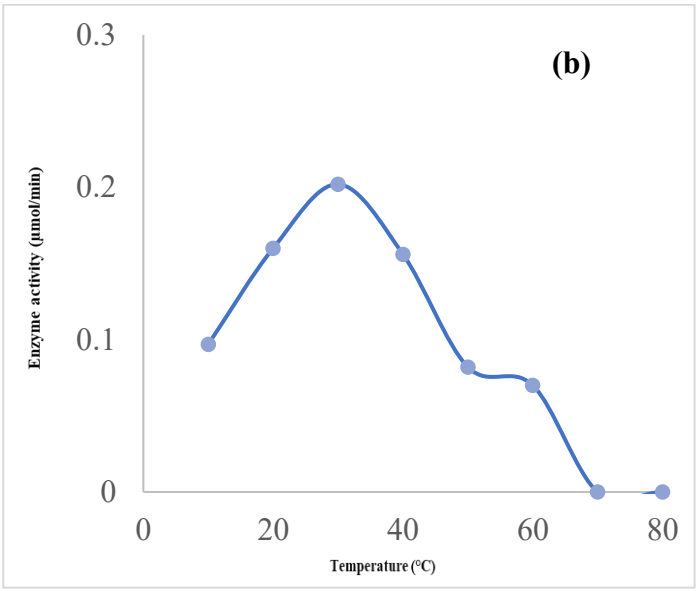


Fig. 7. TOF MS and MS/MS spectra of purified LiP showing the precursor ion and characteristic fragment ions

3.5 Physicochemical Characterization of LiP

The physicochemical profiling of LiP revealed distinct activity patterns under different environmental conditions. The pH–activity profile (Fig. 8a) showed that the enzyme exhibited maximum activity in the acidic range, indicating its suitability for reactions under low pH conditions. Temperature activity studies were conducted to determine the effect of temperature on enzyme activity (Fig 8b). The temperature results showed that the enzyme had an optimum temperature of 30°C and decreased in activity with increasing temperature, which would indicate thermal denaturation sensitivity at temperatures higher than optimum. The enzyme was shown to be affected by buffer concentration (Fig. 8c) and also exhibited maximum enzyme activity at a buffer concentration of 50 mM sodium tartrate. The above results demonstrate the importance of physicochemical factors in the stability and catalytic activity of an enzyme.





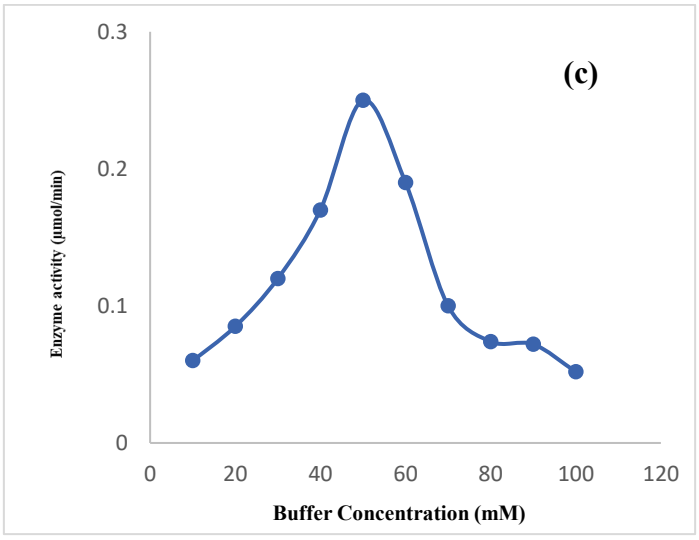
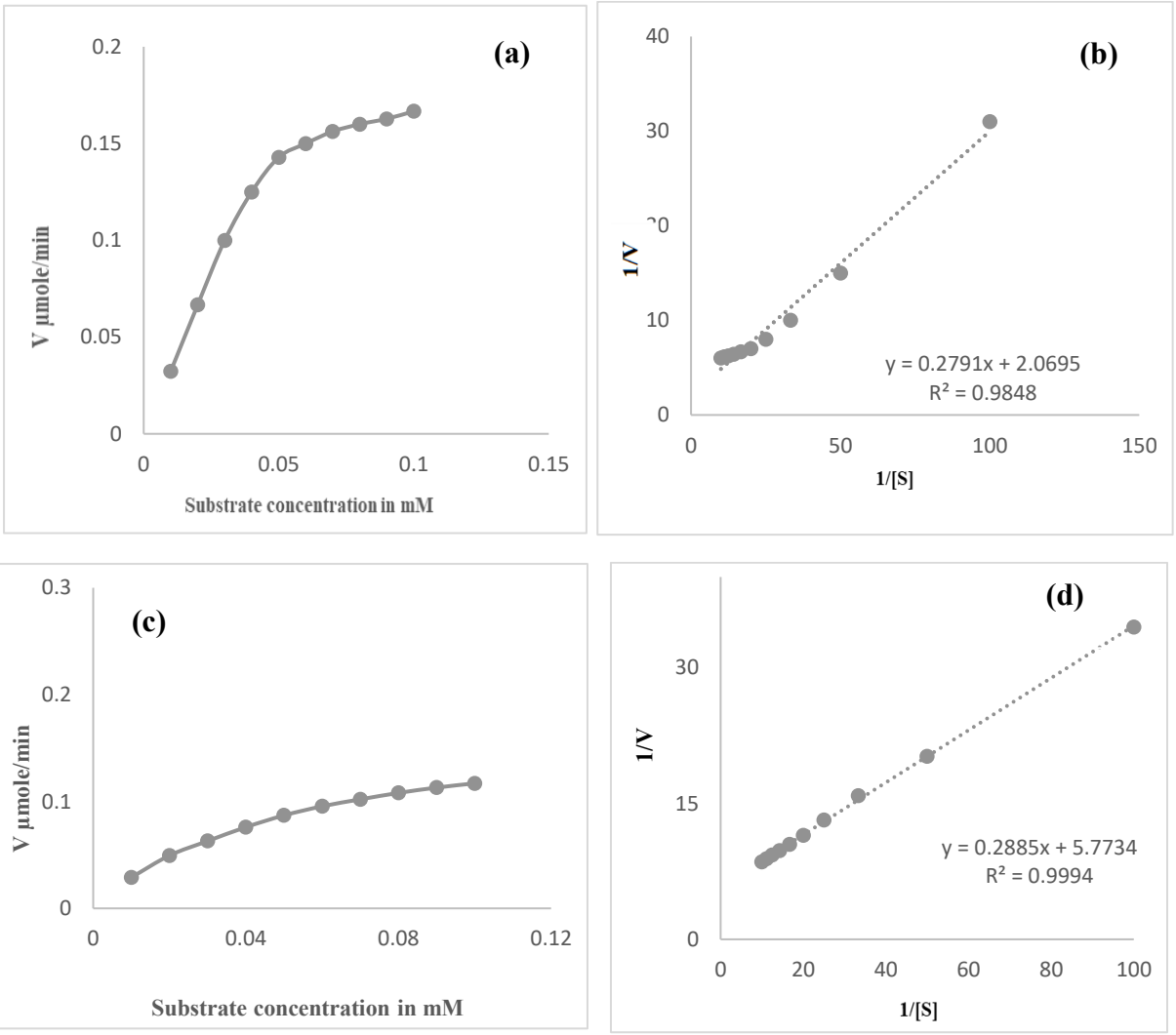


Fig. 8. Effect of physicochemical parameters on the activity of purified LiP (a) effect of pH, (b) effect of temperature, and (c) effect of sodium tartrate buffer concentration on enzyme activity. Data are presented as mean ± SD of three independent experiments.

3.6 Kinetic analysis employing primary and functional substrates

The kinetic properties of purified LiP from *Fusarium odoratissimum* were evaluated using veratryl alcohol, H_2O_2, and n-propanol (Fig. 9a–f) **Table 2**. Veratryl alcohol exhibited a K_m of 135 µM, V_{max} of 0.4832 µmol min^{-1}, and kcat of 23.88 s^{-1}, with a catalytic efficiency of 1.77 × 10^5 M^{-1} s^{-1}. H_2O_2 showed a K_m of 72.1 µM and catalytic efficiency of 1.83 × 10^5 M^{-1} s^{-1}, whereas n-propanol displayed the lowest K_m (60.76 µM) and highest catalytic efficiency (2.27 × 10^5 M^{-1} s^{-1}). These findings indicate high substrate affinity and catalytic efficiency of purified LiP, highlighting its potentialal for biotechnological applications.



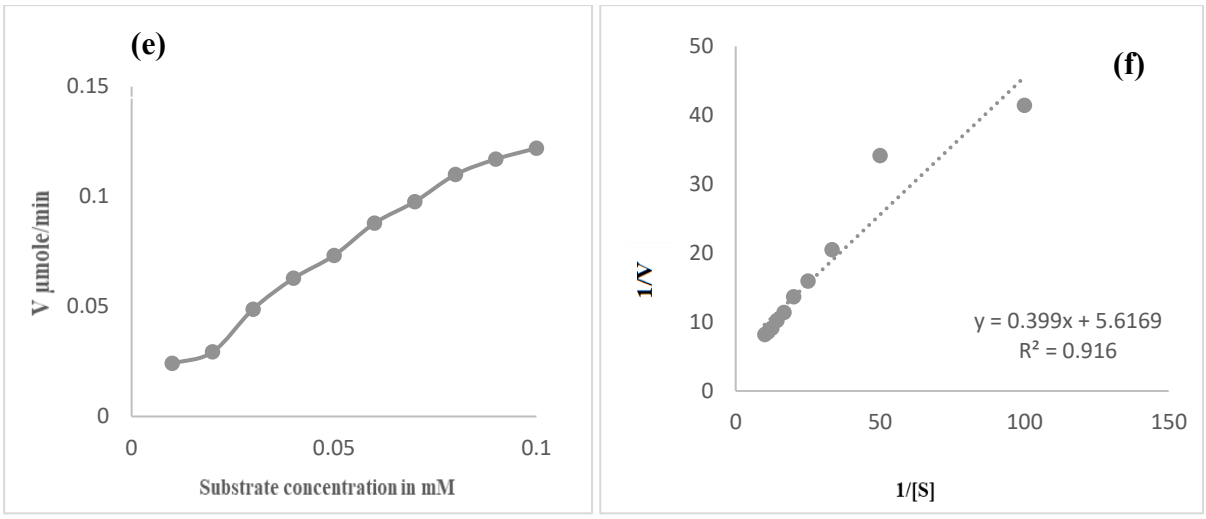


Fig. 9. Michaelis–Menten and Lineweaver–Burk kinetic analyses of purified LiP using (a, b) veratryl alcohol, (c, d) H_2O_2, and (e, f) n-propanol as substrates.

Table 2. Kinetic parameters of LiP with different substrates

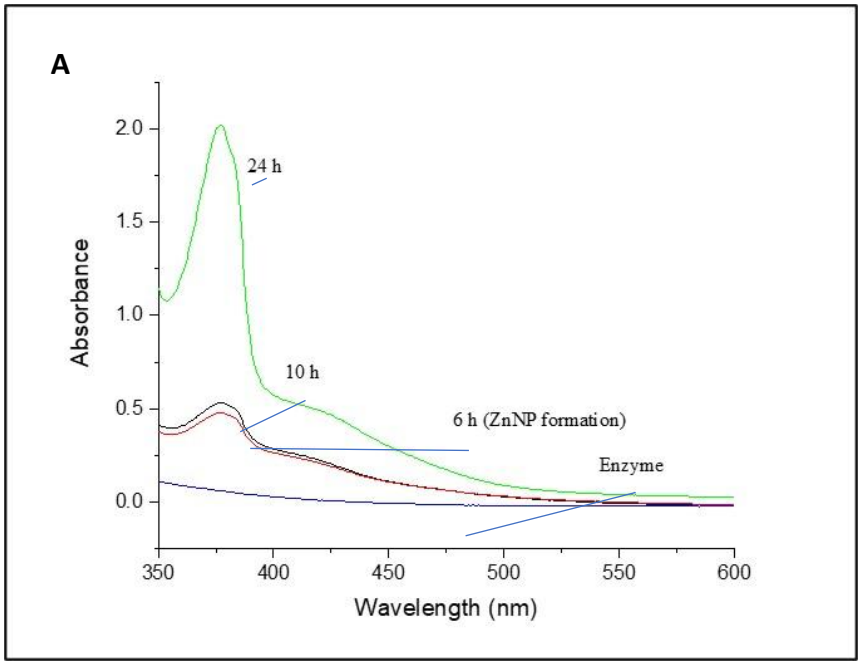
Substrate	K_m (µM)	V_{max} (µmol·min^{-1})	k_{cat} (s^{-1})	k_{cat}/K_m ($M^{-1}\cdot s^{-1}$)
Veratryl alcohol	135.0 ± 4.8	0.4832 ± 0.0125	23.88	1.77×10^5
H_2O_2	72.1 ± 3.1	0.3223 ± 0.0098	13.2	1.83×10^5
n-Propanol	60.76 ± 2.7	0.3364 ± 0.0106	13.78	2.27×10^5

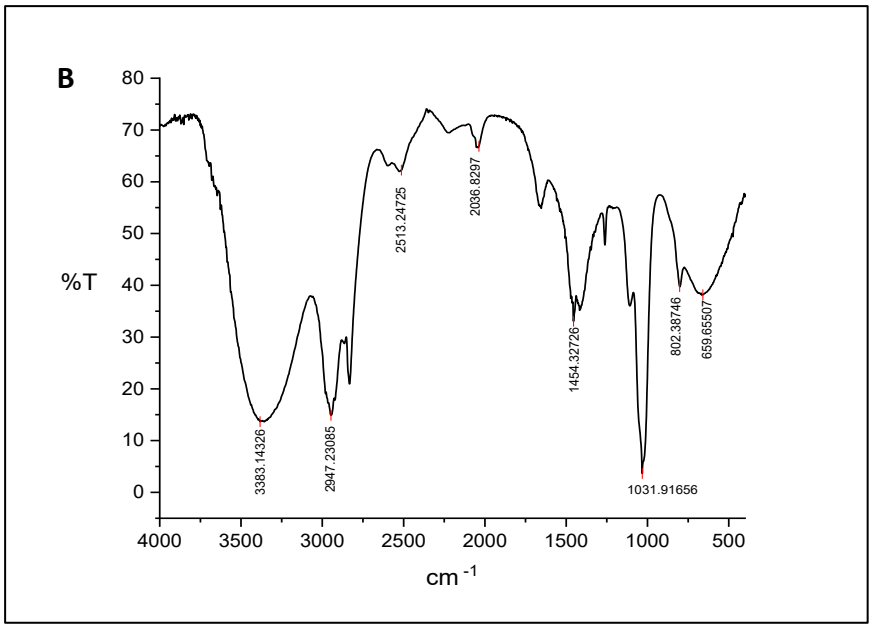
3.7. Synthesis and characterization of LiP-mediated ZnO nanoparticles

The synthesis of ZnO NPs using purified LiP was investigated by UV–Visible spectroscopy, FTIR, EDS, FESEM, particle-size distribution, zeta-potential, DLS, and XRD analyses (Fig. 10). Appropriate control experiments were included to evaluate the contribution of LiP to ZnO nanoparticle formation and to distinguish enzyme-associated nanoparticle formation from spontaneous precipitation or nonspecific protein interactions. The UV–Visible absorption spectrum of the LiP-mediated reaction exhibited a characteristic absorption maximum at approximately 380 nm, with a progressive increase in absorbance with reaction time, indicating the formation of ZnO NPs (Fig. 10a). Spectra were recorded at 6, 10, and 24 h, and the absorption maximum was most pronounced at 24 h. The observed absorption near 380 nm is consistent with the characteristic optical absorption of ZnO nanoparticles. The involvement of LiP in nanoparticle formation may be associated with interactions between Zn^{2+} ions and functional groups present in the enzyme, which may facilitate nucleation and stabilization of the newly formed nanoparticles. FTIR analysis showed characteristic absorption bands corresponding to functional groups present in purified LiP, including hydroxyl, amine, carbonyl, and C–O groups (Fig. 10b). Following ZnO nanoparticle formation, changes in the

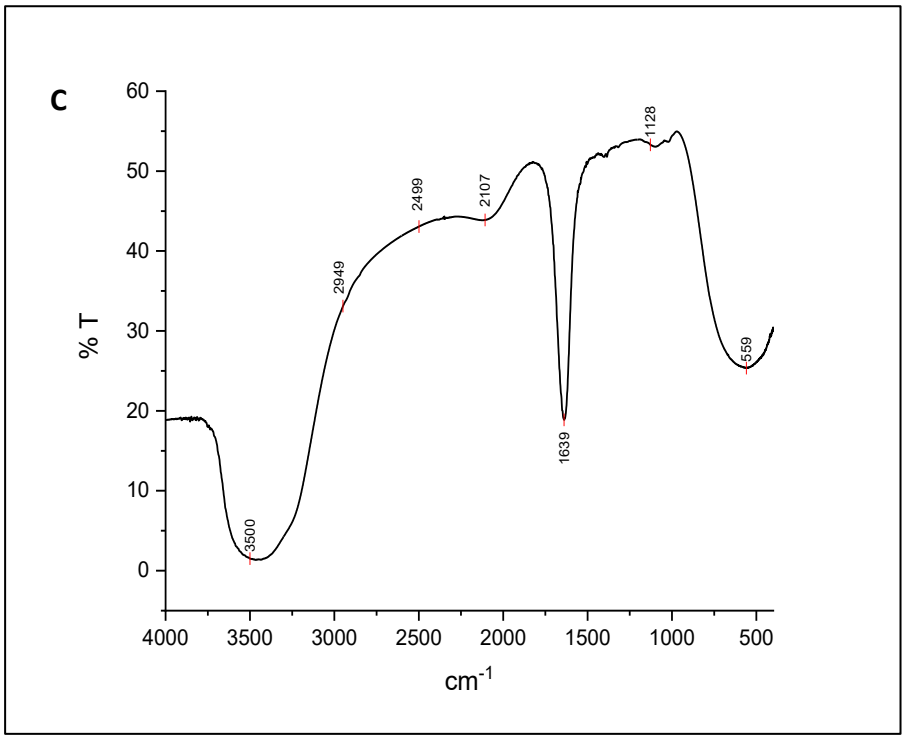
position and intensity of these bands were observed, together with the characteristic Zn–O vibration, suggesting the possible involvement of protein-associated functional groups in the formation and surface stabilization of the nanoparticles (Fig. 10c). These spectral changes indicate interactions between LiP-associated functional groups and the ZnO nanoparticle surface and support the proposed role of the enzyme as a biological facilitator and stabilizing component during nanoparticle synthesis.

EDS analysis confirmed the presence of Zn and O as the predominant elements in the synthesized nanoparticles, with Zn and O contents of 82.66 wt% (52.46 at%) and 17.34 wt% (47.54 at%), respectively (Fig. 10d). The predominance of Zn and O signals supports the formation of ZnO. FESEM analysis revealed predominantly spherical to quasi-spherical nanoparticles with some degree of agglomeration (Fig. 10e, f). The observed particle-size distribution was approximately 20–60 nm, with a greater proportion of particles occurring in the 30–40 nm range (Fig. 10g). The XRD pattern exhibited distinct diffraction reflections characteristic of crystalline ZnO (Fig. 10h). The major reflections were indexed to the (100), (002), (101), (102), (110), (103), (200), (112), and (201) planes, respectively, and were consistent with the hexagonal wurtzite structure of ZnO according to the corresponding ICDD/JCPDS standard reference. Zeta-potential analysis showed an average surface charge of −20.9 ± 24.4 mV, with a dominant peak centred at −23.1 mV (92.5% area) (Fig. 10i). The negative surface charge may be associated with ionized protein-derived functional groups adsorbed on or associated with the nanoparticle surface. The magnitude of the measured zeta potential suggests moderate electrostatic stabilization. DLS analysis showed a Z-average hydrodynamic diameter of 452.7 nm and a polydispersity index (PDI) of 0.470, with a major intensity peak at 240.4 nm (77.7% intensity) (Fig. 10j). The considerably larger hydrodynamic diameter compared with the FESEM-derived primary particle size indicates the presence of particle aggregation in aqueous suspension. Collectively, the spectroscopic, elemental, morphological, surface-charge, particle-size, and crystallographic analyses support the formation of crystalline ZnO nanoparticles through the LiP-mediated synthesis approach.

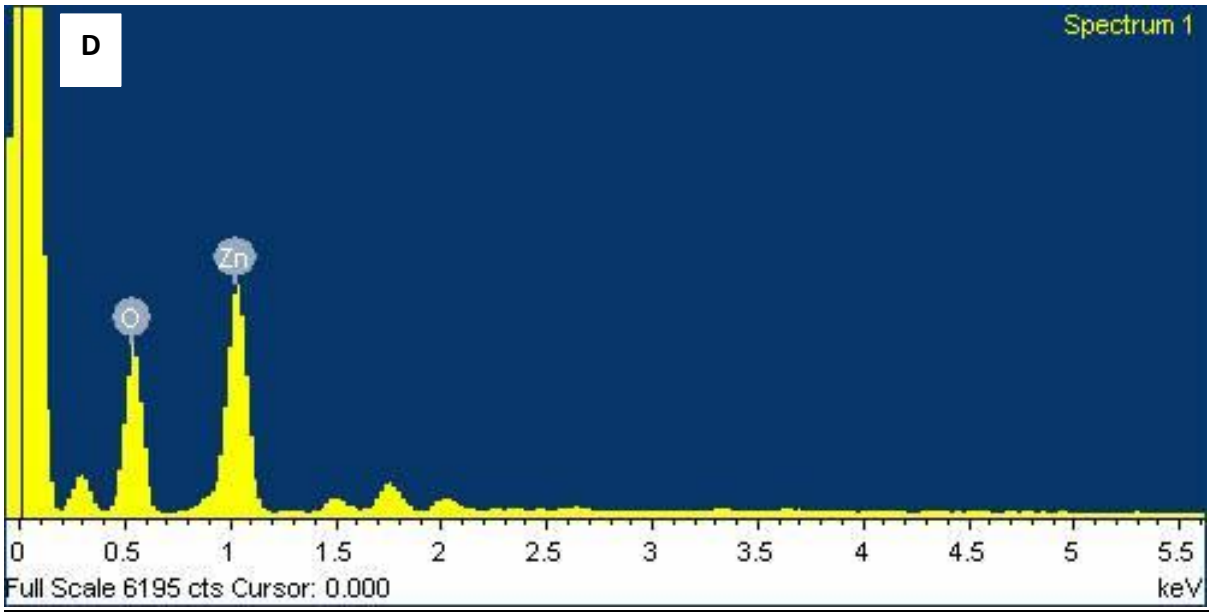



B
%T
cm -1
3383.14326
2947.23085
2513.24725
2036.8297
1454.32726
1031.91656
802.38746
659.65507

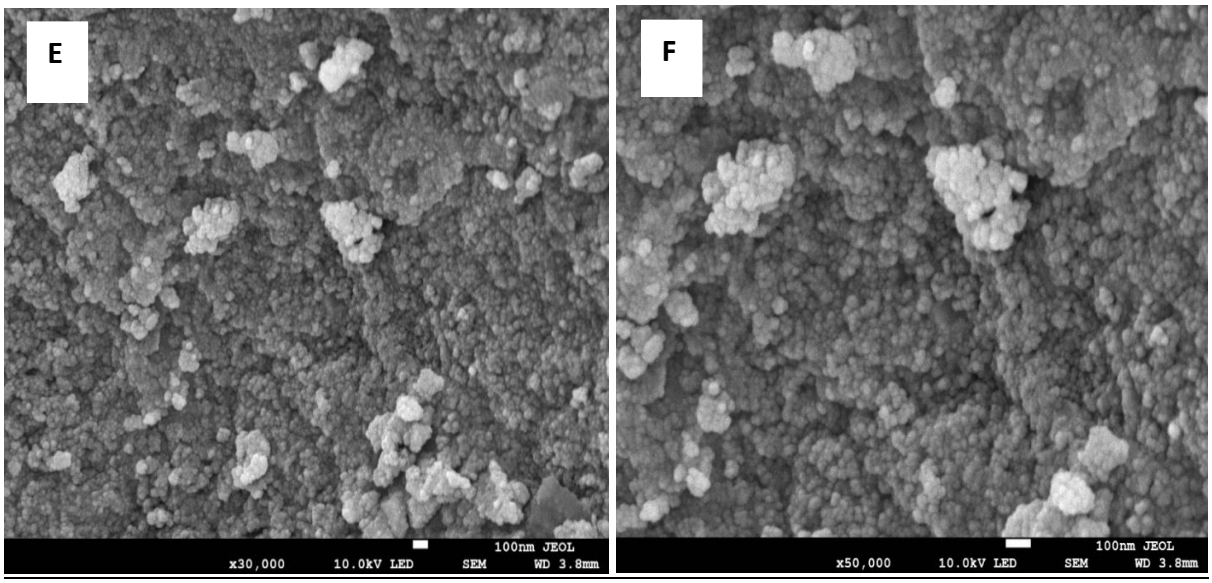
50


C
% T
cm-1
3500
2949
2499
2107
1639
1128
559

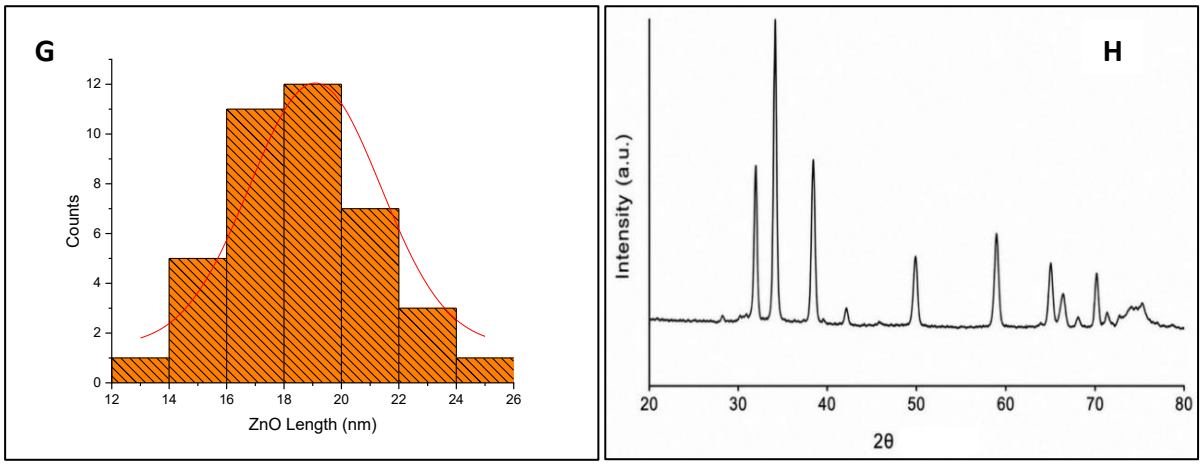
51


D
Spectrum 1
Zn
O
0
0.5
1
1.5
2
2.5
3
3.5
4
4.5
5
5.5
Full Scale 6195 cts Cursor: 0.000
keV

52


E
F
x30,000
10.0kV LED
SEM
WD 3.8mm
100nm JEOL
x50,000
10.0kV LED
SEM
WD 3.8mm
100nm JEOL

53


G
Counts
ZnO Length (nm)
H
Intensity (a.u.)
2θ

54

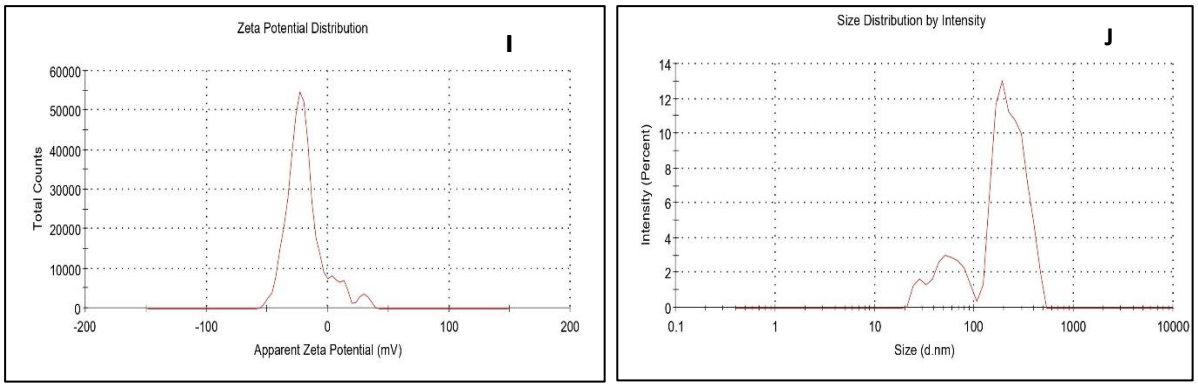


Fig. 10. Characterization of LiP-mediated ZnO nanoparticles by (a) UV–Visible spectroscopy, (b, c) FTIR spectra of purified LiP and LiP-mediated ZnO nanoparticles, (d) energy-dispersive X-ray spectroscopy (EDS), (e, f) FESEM micrographs, (g) XRD pattern, (h) zeta potential distribution, and (i) dynamic light scattering (DLS) particle size distribution.

3.8 Application of LiP-mediated ZnO nanoparticles for BOD and COD removal

Evaluated the potential use of LiP-assisted ZnO nanoparticles in treating Dikrong River water by measuring BOD and COD removals across different doses of nanoparticles and contact times. **Table 3** showed BOD and COD removal efficiencies with respect to different doses of ZnO nanoparticles. Increased ZnO nanoparticle doses (20 to 100 mg) significantly enhanced BOD and COD removals due to additional active sites available for adsorption or catalysis. For example, BOD concentrations fell from 88.1 mg/L to 2.8 mg/L (removal efficiency of 97.0%), while COD concentrations reduced from 575 mg/L to 259 mg/L (removal efficiency of 55.0%). Greater amounts of nanoparticles per unit volume enhanced the interaction between BOD and COD pollutants and nanoparticle surfaces due to additional available adsorption and catalytic sites. Also recorded how long contact times affected pollutant removals (**Table 4**). Increasing the contact time (20 to 100 min) resulted in increased performance of pollutants being removed via BOD from 81.0% to 90.7% and COD from 12.0% to 49.4%. After 100 minutes, BOD and COD concentrations decreased to 8.6 mg/L and 291 mg/L, respectively. The ability to achieve greater BOD and COD removals after prolonged contact times suggests greater interaction between BOD and COD pollutants and nanoparticle surfaces. In conclusion, LiP-mediated ZnO nanoparticles demonstrated superior efficiencies in removing BOD and COD from river waters and had the potential to be utilized as an environmentally friendly nano-material for treating river waters and wastewater.

Table 3. Effect of ZnO nanoparticle dosage on BOD and COD removal

ZnO-NP (mg)	BOD Before (mg/L)	BOD After (mg/L)	BOD Removal (%)	COD Before (mg/L)	COD After (mg/L)	COD Removal (%)
20	88.1 ± 0.1	20.3 ± 0.1	77.0 ± 0.1	575 ± 0.2	421 ± 0.1	26.8 ± 0.1
40	88.1 ± 0.1	15.4 ± 0.1	82.5 ± 0.1	575 ± 0.2	389 ± 0.1	32.3 ± 0.1

60	88.1 ± 0.1	10.9 ± 0.1	87.6 ± 0.1	575 ± 0.2	326 ± 0.1	43.3 ± 0.1
80	88.1 ± 0.1	6.2 ± 0.1	93.0 ± 0.1	575 ± 0.2	292 ± 0.1	49.2 ± 0.1
100	88.1 ± 0.1	2.8 ± 0.1	96.8 ± 0.1	575 ± 0.2	259 ± 0.1	55.0 ± 0.1

Table 4. Effect of contact time on BOD and COD removal

Contact Time (min)	BOD Concentration (mg/L)	BOD Removal (%)	COD Concentration (mg/L)	COD Removal (%)
20	17.5 ± 0.09	81.0 ± 0.10	506 ± 0.12	12.0 ± 0.08
40	15.6 ± 0.08	83.1 ± 0.08	478 ± 0.10	16.9 ± 0.07
60	13.2 ± 0.06	85.7 ± 0.07	418 ± 0.09	27.3 ± 0.05
80	9.2 ± 0.05	90.0 ± 0.05	354 ± 0.08	38.4 ± 0.04
100	8.6 ± 0.04	90.7 ± 0.04	291 ± 0.06	49.4 ± 0.03

3.9 Biological Activities

3.9.1 Radical-Scavenging Activity of LiP-Mediated ZnO NPs

The antioxidant activity of the extracellular enzyme extract and fungal-synthesized ZnO nanoparticles was evaluated using ABTS and DPPH radical-scavenging assays. All measurements were performed in replicates, and the results are expressed as mean ± standard deviation (SD). In both assays, radical-scavenging activity increased progressively with increasing concentration, with the ZnO-NPs showing higher activity than the extracellular enzyme extract (Figs. 11 and 12). A concentration-dependent increase in radical-scavenging activity was observed in the ABTS assay (Fig. 11a,b). The extracellular enzyme extract exhibited an EC_{50} of 144.19 ± 16.2 µg/mL, whereas the fungal-synthesized ZnO-NPs showed a lower EC_{50} of 99.63 ± 11.2 µg/mL (Fig. 11a,b). The lower EC_{50} value of the ZnO-NPs indicates stronger apparent ABTS radical-scavenging activity compared with the extracellular enzyme extract.

A similar trend was observed in the DPPH assay (Fig. 12a,b). The ZnO -NPs exhibited an EC_{50} of 120.2 ± 19.5 µg/mL, compared with 170.2 ± 11.5 µg/mL for the extracellular enzyme extract (Fig. 12a,b). The lower EC_{50} value indicates greater apparent DPPH radical-scavenging activity of the ZnO -NPs. Overall, the ZnO -NPs exhibited lower EC_{50} values in both ABTS and DPPH assays (Figs. 11 and 12), indicating enhanced apparent antioxidant potential compared with the extracellular enzyme extract. This enhancement may be associated with the combined contribution of fungal-derived bioactive metabolites associated with the nanoparticle surface and the physicochemical characteristics of the ZnO nanomaterial. Surface-associated functional

groups may contribute to electron or hydrogen donation during radical neutralization, while the nanoscale structure may facilitate interaction with radical species. Thus, the fungal-synthesized ZnO-NPs demonstrated enhanced apparent radical-scavenging activity under the tested conditions.

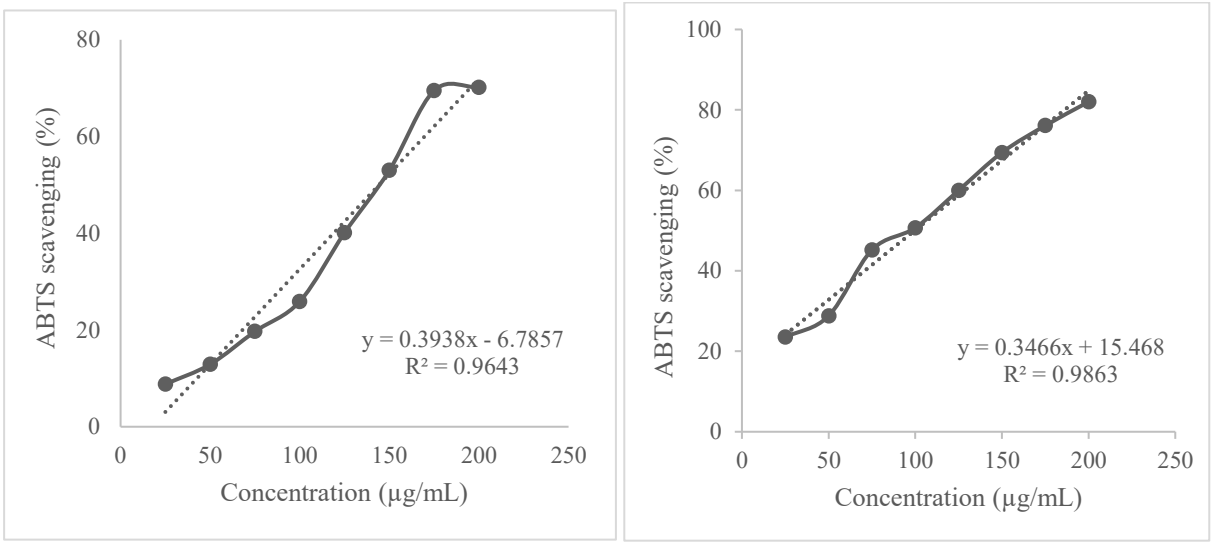


Fig. 11. ABTS radical-scavenging activity of (a) extracellular enzyme extract and (b) ZnO-NPs.

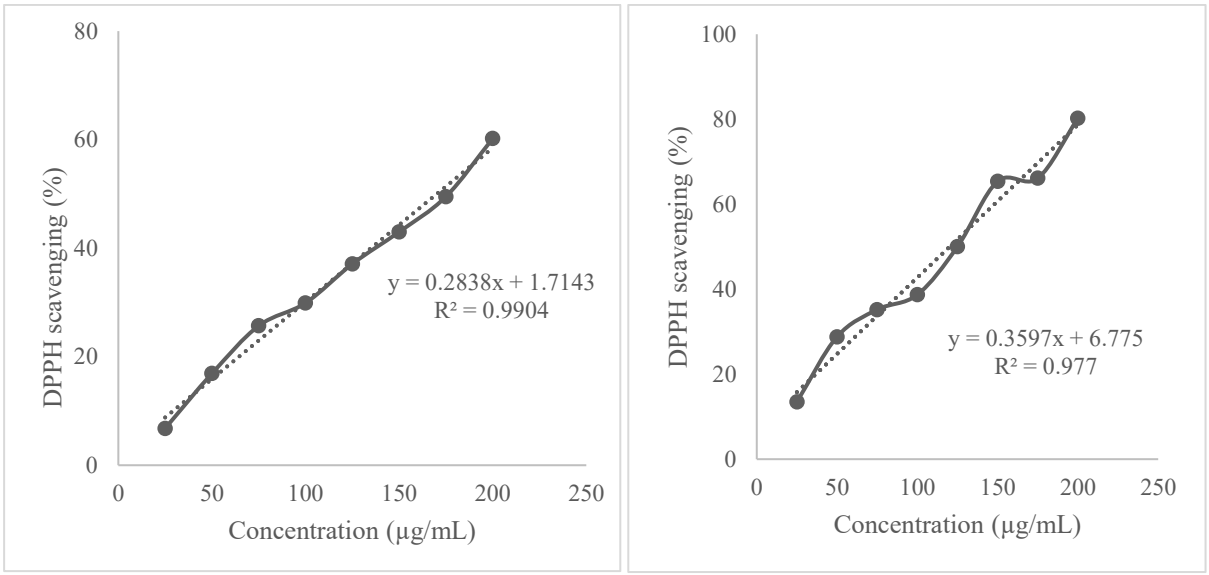
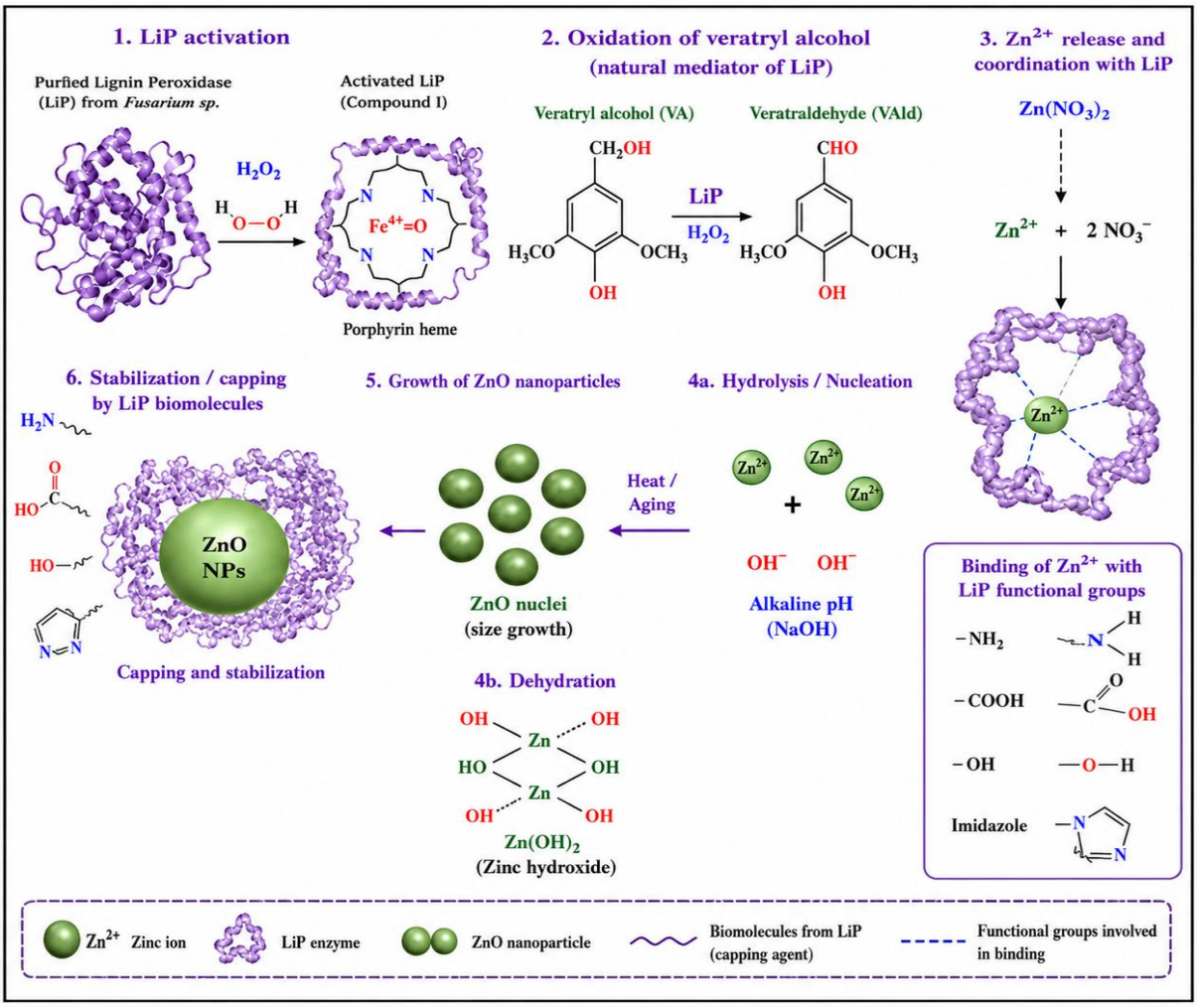


Fig. 12. DPPH radical-scavenging activity of (a) extracellular enzyme extract and (b) ZnO-NPs.

4. Discussion

The present study demonstrated the production, purification, and characterization of LiP from *Fusarium odoratissimum* and its application in enzyme-assisted ZnO nanoparticle synthesis. Purification resulted in an 18.55-fold increase in specific activity, indicating effective enrichment of the enzyme for subsequent application. The synthesized ZnO nanoparticles were characterized by UV–Vis, FTIR, FESEM, EDS, particle-size analysis, zeta potential, DLS, and XRD, confirming the formation of crystalline ZnO with protein-associated surface functional

groups. The proposed synthesis pathway is illustrated in Fig. 13. LiP is activated by H_2O_2 and participates in veratryl alcohol oxidation. Meanwhile, Zn^{2+} released from $Zn(NO_3)_2$ may interact with functional groups associated with LiP, followed by hydroxide formation under alkaline conditions. Subsequent aging and dehydration can promote ZnO nucleation and particle growth. LiP-derived biomolecules may remain associated with the nanoparticle surface and contribute to capping and stabilization. This pathway represents a proposed mechanism; the present experiments do not directly establish electron transfer between veratryl alcohol oxidation and Zn^{2+} or confirm the contribution of individual protein functional groups. The synthesized nanoparticles showed concentration- and contact-time-dependent reductions in BOD and COD of Dikrong River water. At 100 mg, BOD and COD removals reached approximately 96.8% and 55.0%, respectively. These results indicate reduction of oxygen-demanding organic matter but do not by themselves demonstrate complete degradation or mineralization. The nanoparticles also exhibited radical-scavenging activity in ABTS and DPPH assays, with lower EC_{50} values than the extracellular enzyme extract, indicating greater apparent antioxidant activity under the tested conditions. Overall, the findings support LiP-assisted ZnO synthesis and its potential for water-quality improvement and in-vitro radical-scavenging activity.



s

Fig. 13. Proposed mechanism of LiP-mediated ZnO nanoparticle synthesis, illustrating LiP activation, Zn^{2+} coordination, ZnO nucleation, particle growth, and biomolecule-mediated stabilization.

5. Conclusion

The present study demonstrated the production, purification, and application of LiP from *Fusarium odoratissimum* for the enzyme-assisted green synthesis of ZnO nanoparticles. The successful synthesis of ZnO nanoparticles and their demonstrated functional activities highlight the potential of LiP as a biological mediator for sustainable nanoparticle production. As a whole, the research presents the concept proof of ZnO nanoparticle formation supported by LiP and its prospective applications for environmental purposes. The next studies should investigate the molecular mechanism of nanoparticle formation, examine stabilizing properties of nanoparticles including ecotoxicity and fate in the environment, and evaluate its efficiency in simulated wastewater conditions. Moreover, further investigations on the recovery, reusability, and enlarging the scale of the processes will improve understanding of its practical applicability.

Declaration of Competing Interest

The authors declare no conflict of interest or relations.

Data Availability

The data used in this study can be sourced from the corresponding author upon request.

Acknowledgements

The authors express their gratitude to the Department of Chemistry of North Eastern Regional Institute of Science and Technology (NERIST), Nirjuli, Arunachal Pradesh, India, for providing the necessary facilities for completion of this work.

Funding

The authors received no specific funding for this work.

References

American Public Health Association. Standard methods for the examination of water and wastewater. American Public Health Association.; 1926.

Anuar MS, Khairuddin NH, Zainal ZS, Nazarudin MF, Azmai MN, Salleh A, Abdullah CA, Yasin IS, Yusof MT. Lecanicillium coprophilum–mediated green synthesis of zinc oxide nanoparticles displaying antimicrobial activity against important rice pathogens. Mycologia. 2025 Sep 3;117(5):801-17.

Aragaw TA, Bogale FM, Gessesse A. Adaptive response of thermophiles to redox stress and their role in the process of dye degradation from textile industry wastewater. Frontiers in Physiology. 2022 Jun 20;13:908370.

Biko OD, Viljoen-Bloom M, van Zyl WH. Microbial lignin peroxidases: applications, production challenges and future perspectives. Enzyme and Microbial Technology. 2020 Nov 1;141:109669.

Borang N, Dutta A, Yadav M. Lignin valorisation into functional nanocarriers and nanoparticle-enabled enzyme immobilisation: Emerging strategies for sustainable detoxification of agroecosystems. Biocatalysis and Biotransformation. 2026 Jun 26:1-20.

Bouacem K, Rekik H, Jaouadi NZ, Zenati B, Kourdali S, El Hattab M, Badis A, Annane R, Bejar S, Hacene H, Bouanane-Darenfed A. Purification and characterization of two novel peroxidases from the dye-decolorizing fungus Bjerkandera adusta strain CX-9. International Journal of Biological Macromolecules. 2018 Jan 1;106:636-46.

Elisashvili V, Kachlishvili E. Physiological regulation of laccase and manganese peroxidase production by white-rot Basidiomycetes. Journal of biotechnology. 2009 Oct 12;144(1):37-42.

El-Saadony MT, Fang G, Yan S, Alkafaas SS, El Nasharty MA, Khedr SA, Hussien AM, Ghosh S, Dladla M, Elkafas SS, Ibrahim EH. Green synthesis of zinc oxide nanoparticles: preparation, characterization, and biomedical applications-a review. International journal of nanomedicine. 2024 Dec 31:12889-937.

Gomaa EZ. Microbial mediated synthesis of zinc oxide nanoparticles, characterization and multifaceted applications. Journal of Inorganic and Organometallic Polymers and Materials. 2022 Nov;32(11):4114-32.

Hashempour Y, Mortezazadeh F, Rezaei S, Salehipour M, Gholami-Borujeni F, Ebrahimnejad P, Mogharabi-Manzari M. Co-immobilization of laccase and zinc oxide nanoparticles onto bacterial cellulose to achieve synergistic effect of photo and enzymatic catalysis for biodegradation of favipiravir. International Journal of Biological Macromolecules. 2025 Mar 1;292:139288.

Laemmli UK. Cleavage of structural proteins during the assembly of the head of bacteriophage T4. Nature. 1970 Aug;227(5259):680-5.

Lineweaver, H. and Burk, D., 1934. The determination of enzyme dissociation constants. *Journal of the American chemical society*, *56*(3), pp.658-666.

Lowry OH, Rosebrough NJ, Farr AL, Randall RJ. Protein measurement with the Folin phenol reagent. J Biol Chem. 1951 Jul;193(1):265-75.

Mazumder JA, Ahmad A, Ali J, Noori R, Bhuyan T, Sardar M, Sheehan D. Biomimetic green synthesis of ZnO nanoflowers using α-amylase: from antimicrobial to toxicological evaluation. Scientific Reports. 2024 Jul 17;14(1):16566.

Murali M, Gowtham HG, Shilpa N, Singh SB, Aiyaz M, Sayyed RZ, Shivamallu C, Achar RR, Silina E, Stupin V, Manturova N. Zinc oxide nanoparticles prepared through microbial mediated synthesis for therapeutic applications: A possible alternative for plants. Frontiers in microbiology. 2023 Sep 5;14:1227951.

Nehru L, Kandasamy GD, Sekar V, Alshehri MA, Panneerselvam C, Alasmari A, Kathirvel P. Green synthesis of ZnO-NPs using endophytic fungal extract of Xylaria arbuscula from Blumea axillaris and its biological applications. Artificial Cells, Nanomedicine, and Biotechnology. 2023 Dec 31;51(1):318-33.

Parveen S, Asgher M, Bilal M. Lignin peroxidase-based cross-linked enzyme aggregates (LiP-CLEAs) as robust biocatalytic materials for mitigation of textile dyes-contaminated aqueous solution. Environ Technol Innov. 2021 Dec; 21:101226.

Pointing S. Feasibility of bioremediation by white-rot fungi. Applied microbiology and biotechnology. 2001 Oct;57(1):20-33.

Rani M, Shanker U. Removal of organic dyes by functionalized nanomaterials. In: Handbook of Green and Sustainable Nanotechnology: Fundamentals, Developments and Applications. Cham: Springer International Publishing; 2022. p.1-32.

Sharma JL, Dhayal V, Sharma RK. Antibacterial effect of glycerol assisted ZnO nanoparticles synthesized by white rot fungus Phanerochaete chrysosporium. Materials Today: Proceedings. 2021 Jan 1;43:2855-60.

Sharma JL, Dhayal V, Sharma RK. White-rot fungus mediated green synthesis of zinc oxide nanoparticles and their impregnation on cellulose to develop environmental friendly antimicrobial fibers. 3 Biotech. 2021 Jun;11(6):269.

Sharma R, Garg R, Kumari A. A review on biogenic synthesis, applications and toxicity aspects of zinc oxide nanoparticles. EXCLI journal. 2020 Sep 22;19:1325.

Shi N, Cheng D, Chen Y, Feng Y, Saeed M, Guo Z, Hu Z, Chen H. Improvement in lignin peroxidase oxidative stability via surface display by Bacillus subtilis. Biotechnol Lett. 2025;47(4):1-13.

Singh AK, Bilal M, Iqbal HM, Raj A. Lignin peroxidase in focus for catalytic elimination of contaminants—A critical review on recent progress and perspectives. International Journal of Biological Macromolecules. 2021 Apr 30;177:58-82.

Singh AK, Fernandez-Lafuente R, Schmidt JE, Boczkaj G, Bilal M. Biocatalytic functionalities of lignin peroxidase-based systems in lignin depolymerization and pollutants removal from environmental matrices. Curr Pollut Rep. 2024 Sep;10(3):345-61.

Singh R, Shedbalkar UU, Nadhe SB, Wadhwani SA, Chopade BA. Lignin peroxidase mediated silver nanoparticle synthesis in Acinetobacter sp. Amb Express. 2017 Dec 22;7(1):226.

Sus B, Baltaci MO, Nadaroglu H, Adiguzel A. From agro-food waste to nanoparticles: green synthesis of copper nanoparticles with lignin peroxidase enzyme produced by Anoxybacillus rupiensis using peanut shells. Environmental Science and Pollution Research. 2024 Aug;31(39):52049-59.

Thulasisingh A, Ananthakrishnan K, Raja A, Kannaiyan S. Bioprospecting of novel and industrially appropriate enzymes: A review. Water Air Soil Pollut. 2024 Jan;235(1):12.

Tien M, Kirk TK. Lignin-degrading enzyme from Phanerochaete chrysosporium: purification, characterization, and catalytic properties of a unique H2O2-requiring oxygenase. Proceedings of the National Academy of Sciences. 1984 Apr;81(8):2280-4.

Vignati DA, Lofrano G, Libralato G, Guida M, Siciliano A, Carraturo F, Carotenuto M. Photocatalytic ZnO-assisted degradation of spiramycin in urban wastewater: Degradation kinetics and toxicity. Water. 2021 Apr 11;13(8):1051.

Wesenberg D, Kyriakides I, Agathos SN. White-rot fungi and their enzymes for the treatment of industrial dye effluents. Biotechnol Adv. 2003 Jan-Feb;22(1-2):161-87.

Wheelwright SM. Protein purification: design and scale up of downstream processing. (No Title). 1991 Jan.

Worthington Biochemical Corporation (Freehold NJ). Worthington enzyme manual: enzymes, enzyme reagents, related biochemicals. Worthington Biochemical Corporation; 1972.

Supplementary Files

This is a list of supplementary files associated with this preprint. Click to download.

- SupplementaryFileS1.pdf